Journal of
Synchrotron
Radiation

ISSN 0909-0495

Received 14 April 2005
Accepted 14 July 2005

# Quantitative high-pressure pair distribution function analysis

**John B. Parise,[a,b]* Sytle M. Antao,[b] F. Marc Michel,[a,b] C. David Martin,[b] Peter J. Chupas,[c] Sarvjit D. Shastri[d] and Peter L. Lee[d]**

[a]Center for Environmental Molecular Sciences, CEMS, Stony Brook, NY 11794, USA, [b]Department of Geosciences, State University of New York, Stony Brook, NY 11794, USA, [c]Materials Science Division, MSD 223, Argonne National Laboratory, Argonne, IL 60439, USA, and [d]XOR, Advanced Photon Source, Argonne National Laboratory, Argonne, IL 60439, USA.
E-mail: john.parise@stonybrook.edu

The collection of scattering data at high pressure and temperature is now relatively straightforward thanks to developments at high-brightness synchrotron radiation facilities. Reliable data from powders, that are suitable for structure determination and Rietveld refinement, are routinely collected up to about 30 GPa in either a large-volume high-pressure apparatus or diamond anvil cell. In those cases where the total elastic scattering is of interest, as it is in the case of nano-crystalline and glassy materials, technical developments, including the use of focused high-energy X-rays (>80 keV), are advantageous. Recently completed experiments on nano-crystalline materials at the 1-ID beamline at the Advanced Photon Source suggest that quantitative data, suitable for pair distribution function analysis, can be obtained.



**Keywords: high pressure; diffraction; pair distribution function; nano-crystalline materials; diamond anvil cell; perforated diamonds.**

## 1. Introduction

Many of the compounds of interest to materials and earth scientists undergo phase transitions at high pressure. These transitions often involve large changes in structure and in physical properties. Determination of the structure–property relationships must begin with an accurate and precise determination of the atomic parameters, and the changes in these parameters as a function of both pressure ($P$) and temperature ($T$). The determination of crystal structure *ab initio* using high-$P$ powder diffraction data is, in principle, no more difficult than the determination of crystal structure from data collected at ambient conditions. The pressure cell required to maintain high-$P$ conditions usually imposes a number of compromises, however (Parise, 2004). An exception to this is the carefully constructed gas-$P$ apparatus (Jorgensen *et al.*, 1999). Typically, parasitic scattering from the $P$ cell, peak broadening, asymmetry and peak-shifts owing to deviatoric stresses, and several other systematic errors, all compromise data quality. Because of its inherently lower signal-to-background discrimination, the powder diffraction experiment suffers disproportionately from these artifacts, when compared with the single-crystal experiment.

The use of single-crystal diffraction may in fact be the way forward for crystallography at megabar pressure and this aspect is covered extensively in this volume. Working with nano-crystalline or glassy materials at high $P$ on the other hand ensures good powder averaging. Apart from improving powder statistics, there are fundamental questions to be addressed in studying the high-$P$ behavior of nano-crystalline materials, including the influence of surface reconstruction on compressibility and physical properties. Several scattering studies (Lipinska-Kalita *et al.*, 2003; Chen *et al.*, 2002; Wang & Saxena, 2002; Wang *et al.*, 2001*a*,*b*) have addressed the behavior of nano-materials at high $P$, but none provided quantitative crystallographic data that address the problem of deriving reliable structure models for the short-range order in these materials at high $P$. We have made a start on this problem in a series of recent experiments using high-brightness high-energy X-ray scattering (Martin *et al.*, 2005). In order to study aspects of short-range order it is important that not only Bragg scattering be considered in the analysis but that the total elastic scattering, including the diffuse scattering component, be included as well. In the examples below, we review some of our recent work with the diamond anvil cell (DAC) aimed at collecting data suitable for the study of the total scattering from nano-crystalline materials at high $P$.

## 2. Quantitative Rietveld and total scattering studies at high *PT*

In order to monitor changes in short-range order, total scattering studies are now routinely performed at ambient $P$ (Egami & Billinge, 2003). Many of the recent developments in

beamline optics and detectors, which make the collection of high-*PT* data suitable for Rietveld refinement possible, can be used for total scattering from powders as well. For example, the use of point counters with well collimated incident and diffracted beams will exclude much of the parasitic scattering from high-*P* cells (Zhao *et al.*, 1994). Even at high-brightness sources this requires long data collection times (Chen *et al.*, 2001); practically all monochromatic high-*PT* data from powders is now collected using area detectors, imaging plates (IP) or charge coupled devices (CCD).

The use of area detectors usually precludes the use of diffracted beam collimation. This is not so problematic for diamond cell studies where contributions by Bragg scattering from single-crystal diamond anvils can be excluded *ex post facto* using software such as *Fit2D* (Hammersley *et al.*, 1996); the loss of information on the area detector is not so severe since integration around the Debye rings provides sufficient statistics. Some difficulty arises in the case of large-volume high-pressure devices (LVHPD) where components in the beam tend to give rise to parasitic scattering around the whole Debye ring (Chen *et al.*, 1998, 2000). When measurement of the diffuse elastic contribution to the pattern is important, as it is for total scattering, subtraction techniques may eliminate the diffuse scattering component. For this reason, use of a radial collimator (Mezouar *et al.*, 2002) along with a large sample size in a LVHPD is advantageous for quantitative studies of glassy and cryptocrystalline materials.

## 3. Prospects for quantitative high-pressure pair distribution function analysis

### 3.1. Background

While analysis of Bragg diffraction allows us to determine the average crystal structure, in disordered materials, or in ordered nano-crystalline materials, a significant component of diffuse scattering is often ignored or folded into a background correction in the Rietveld methodology. For determination of structural information in disordered or amorphous materials, full-profile fitting of the pair distribution function (PDF) has proven a powerful alternative technique, and is routinely performed using data collected at ambient *P* (Egami & Billinge, 1994; Petkov *et al.*, 2002; Billinge, 2004; Proffen *et al.*, 1999). The atomic PDF, $G(r)$ is defined as

$$G(r) = 4\pi r\big[\rho(r) - \rho_0\big],$$

where $\rho(r)$ and $\rho_0$ are the local and average atomic number densities, respectively, and $r$ is the radial distance. $G(r)$ is then the probability of finding an atom at a distance $r$ from a reference atom and so is related to the atomic structure. $G(r)$ is derived by Fourier transforming the experimentally observed total structure factor (Wasada, 1980), $S(Q)$,

$$G(r) = (2/\pi)\int_{Q=0}^{Q_{\max}} Q[S(Q) - 1]\sin(Qr)\,\mathrm{d}Q,$$

where $Q$ is the magnitude of the wavevector [$Q = 4\pi\sin(\theta)/\lambda$]. The above equation implies that the total scattering, and not just the Bragg scattering, contributes to $G(r)$. Both the long-range order, giving rise to sharp Bragg reflections in the diffraction patterns of crystalline materials, and the short-range order, giving rise to diffuse scattering, are reflected in the PDF. Further, the PDF can serve as a basis for structure refinement and, perhaps, structure determination (Petkov *et al.*, 1999, 2002).

Because of the nature of the scattering from nano-crystalline materials, particularly the lack of sharp Bragg diffraction features, the discrimination between closely related structure models, especially from the compromised data available from high-*P* devices, may be more problematic. Other considerations include (i) the importance of separating out the coherent scattering from incoherent scattering contributions; diamonds, of course, if they are in the beam, will contribute considerable incoherent Compton scattering; and (ii) the need to collect data to as high a value of $Q$ as possible to avoid Fourier termination errors which will show up as ripples in the PDF. Once derived, a properly normalized PDF can be used in a 'Rietveld-like' refinement. A model structure is constructed and the PDF derived from this model. Atomic positions, displacement parameters, occupancies and other model-dependent parameters are then varied to improve the fit between observed and calculated PDF (Egami & Billinge, 2003).

The PDF, which is the measure of the probability of finding atom pairs separated by distance $r$, is also a means of measuring the primary particle size for nano-particles (Fig. 1). For highly crystalline materials the largest distance observable is limited by the instrument resolution, and for crystalline

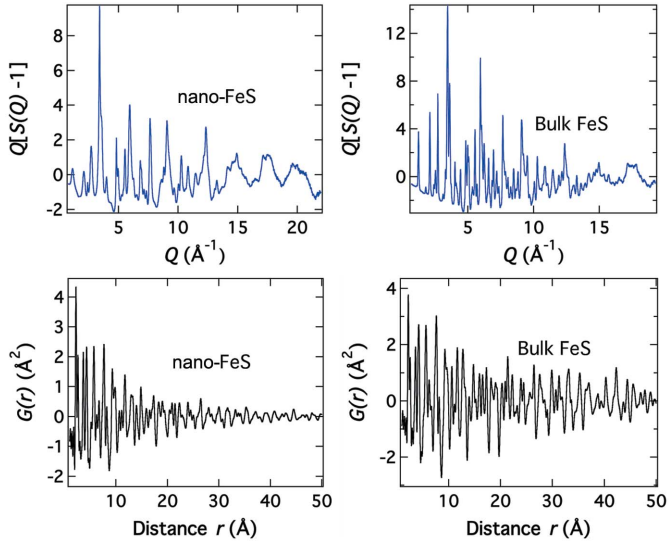


**Figure 1**
Comparison of $Q[S(Q) - 1]$, derived from scattering data collected on an imaging plate (Fig. 2) using 100 keV X-rays at beamline 1-ID, and $G(r)$ plotted out to 50 Å to illustrate the degree of attenuation owing to the range of structural coherence, *i.e.* fundamental particle size, of a nano-crystalline sample of FeS (nano-FeS) and a crystalline sample of FeS (bulk FeS). Determination of fundamental particle size of the crystalline FeS is limited by the instrument resolution, which does not extend beyond ~14 nm, but clearly the correlations in $G(r)$ for nano-FeS are severely attenuated after about 4 nm.

materials such as bulk FeS (Fig. 1) this extends beyond 50 Å. For nano-crystalline materials, such as the freshly precipitated FeS sample (Fig. 1), the PDF is severely attenuated above about 4 nm. This is because, beyond 4 nm for the FeS particles, only intra-particle distances, those <4 nm, would be observed. The behavior of nano-materials under $P$ is of topical interest (Lipinska-Kalita *et al.*, 2003; Chen *et al.*, 2002; Wang & Saxena, 2002; Wang *et al.*, 2001*a*,*b*) and being able to determine the primary particle size, at room and at high $P$, is clearly a first step to characterization.

### 3.2. Deriving PDF from high-*P* data for heavy scatterers

Acquiring scattering data suitable for PDF analysis at high $P$ has primarily required the use of large-volume apparatus as opposed to the DAC. Both high-$P$ cells are subject to considerable parasitic background contributions and narrow $2\theta$ scattering windows, which introduce significant noise to the structure function, $S(Q)$, and final PDF [$G(r)$]. Increasing the $2\theta$ range of data collection and/or scattering vector ($Q$) by increasing the energy of incident radiation improves data quality and eliminates the need for PDF reconstruction, such as Kaplow-type iterative procedures, which force the distribution function to expected values (Shen *et al.*, 2003; Eggert *et al.*, 2002), introducing experimenter bias.

In an initial trial experiment we chose an 'ideal' case to test the viability of using high-energy X-rays to perform quantitative high-pressure pair distribution function (QHP-PDF) analysis: gold with a particle size of 50–100 nm, which gives relatively sharp diffraction features (Fig. 2). The purpose of this initial study was to explore the viability of corrections to the collected diffraction data and the suitability of these data for deriving PDFs for full fitting of structure models. The structure model in this case can be fitted with both Rietveld and with PDF methodologies and so direct comparison can be made of the results. We collected high-energy monochromatic X-ray scattering below the Au edge [79.9562 (5) keV; 0.15507 (3) Å] at the 1-ID beamline of the Advanced Photon Source (APS) at Argonne National Laboratory with 50 µm × 50 µm beam defined by slits. The sample, contained in a standard Merril–Bassett-type DAC, was compressed hydrostatically using an alcohol pressure medium of methanol: ethanol (4:1). Pressure was determined by the ruby fluorescence technique.

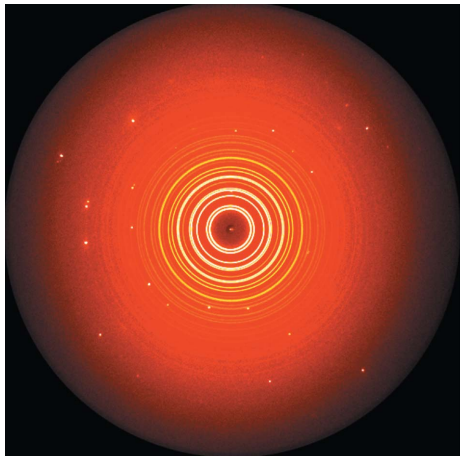

**Figure 2**
Typical exposure on a MAR345 imaging plate illustrating the single-crystal diamond spots alongside powder diffraction from gold held at 8.5 GPa in a DAC. These spots must be carefully masked prior to data integration.

For our initial measurements we find that scattering to 20 $Å^{-1}$ (Petkov *et al.*, 1999) is sufficient for high-quality PDFs of crystalline gold (Martin *et al.*, 2005). Full details of our experimental set-up are reported elsewhere (Martin *et al.*, 2005) but certain aspects are worth repeating here, since the possibility of using nano-phased materials for QHP-PDF holds great promise. In principle the protocols used for the initial study are straightforward and many synchrotron beamlines have the necessary set-up to perform these measurements.

Diffraction patterns were collected using a MAR345 imaging-plate detector. Data treatment included subtraction of background, determined from exposures at ambient $P$ without the sample in position, and exclusion of single-crystal diamond spots, followed by integration with *Fit2D* (Hammersley *et al.*, 1996). To avoid saturation of the detector on any single exposure, and to obtain optimal counting statistics, data were obtained by averaging many short exposures. Typically, data were collected for ten 5 s exposures, which were averaged to attain optimum counting statistics. Integrated data were processed to PDFs using the program *PDFgetX2* (Qiu *et al.*, 2004), where standard corrections as well as those unique to the image-plate geometry were applied (Chupas *et al.*, 2003). Full profile fitting of the PDF was performed using program *PDFFIT* (Proffen & Billinge, 1999), while the program *EXPGUI* (Toby, 2001) for *GSAS* (Larson & Von Dreele, 2000) was used for Rietveld analysis of Bragg diffraction, in order to compare refined model parameters, which are discussed fully in our previous work (Martin *et al.*, 2005).

Several potential pitfalls are avoided by looking at a heavy scatterer such as gold in this initial trial (Martin *et al.*, 2005). The coherent scattering contributions from the methanol: ethanol (4:1) pressure-transmitting medium at 80 keV are small compared with gold. In addition, significantly less pressure-transmitting medium is in the beam than Au sample. The correlations from the alcohol pressure medium must exist and will become more obvious when light elements are used. This will require some combination of samples being loaded in He, elimination of the pressure medium, perhaps along with heating of the sample to eliminate deviatoric stress, and the collection and proper normalization of blanks for subtraction of the pressure-medium contribution. More problematic are contributions from the incoherent scattering of diamond and the severe limitations placed on the brilliance of the beam by using slits rather than an appropriate focusing optic.

### 3.3. Recent modifications to the experimental set-up

While the protocol described above works well for heavy scatterers, for lighter scatterers it is essential to properly

correct for background to remove long-wavelength errors in $S(Q)$, which will Fourier transform into physically meaningless peaks in the low-$r$ (Å) region of the PDF. Tests of the validity of our background correction included comparison of PDFs obtained from gold in a capillary *versus* gold in the DAC at ambient $P$; we found that the difference in PDF between the capillary and DAC is minimal. In the case of heavy scatterers such as gold, we conclude that the background correction is indeed valid and that the data obtained from scattering from crystalline gold are of sufficient quality to allow the derivation of quantitative and well normalized PDFs.

The significant contribution to the background from diamond will need to be addressed (Martin *et al.*, 2005) for studies of glasses, melts and light elements, since in these cases Compton scattering can overwhelm the signal of interest. One solution is to maximize sample size while not compromising $P$ capabilities and, in cases where $P > 35$ GPa is required, larger-volume gem anvil cells are currently under development for neutron sources (Xu *et al.*, 2002). These new devices allow a large sample volume to be taken to pressures above 35 GPa. In those cases where the sample is sufficiently large to allow tight collimation, the problem of Compton and parasitic scattering from high-$P$ cell components is greatly reduced.

Another alternative that will increase the signal-to-noise discrimination is to decrease the inelastic signal by removing some of the diamond from the beam path using perforated diamond anvils (Dadashev *et al.*, 2001) with the geometry shown in Fig. 3. In this case, a conical hole of about 0.5 mm maximum and 80 µm minimum diameter is perforated into the diamond to within 200 µm of the 350 µm-culet. A similar hole is made into the diamond located towards the detector and a miniature anvil set upon it. Providing a beam can be introduced down the hole, in the direction of the arrow in Fig. 3, Compton scattering can be significantly reduced. It is important in this case to focus the incident beam rather than to use beam slits to define the beam size. This maximizes the X-ray flux on the sample. Beamline optics at beamline 1-ID at the APS are well matched to the studies of nano-crystalline and glassy materials at high $PT$. Focused X-rays with energies in the 80–120 keV range provide data to $Q > 20$ Å$^{-1}$ with standard imaging-plate geometries, while minimizing background from the DAC.

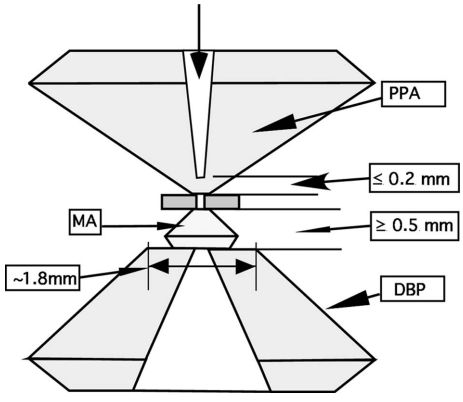


**Figure 3**
A schematic drawing of a DAC with perforated anvils. DBP: diamond backing plate made of ~0.25 carat diamond. Upper conical hole cut to accommodate diameter of incoming beam. PPA: partial perforated anvil made of 0.25 carat diamond with a conical hole. MA: miniature anvil made of ~0.05 carat diamond.

The high-energy X-rays at beamline 1-ID are delivered by a bent double-Laue monochromator followed by vertically focusing refractive lenses. The liquid-nitrogen-cooled monochromator (Shastri *et al.*, 2002) consists of two bent Si(111) Laue crystals arranged to sequential Rowland conditions and provides high flux in a beam of preserved source brilliance (divergence and size). The focusing refractive lenses, placed immediately after the monochromator, are of either the cylindrical aluminium (Shastri, 2004) or saw-tooth silicon (Cederstrom *et al.*, 2002) types, giving line foci of 16–80 µm in vertical size at the end-station, with flux density gains in the range 6–20. A comparison of data collected with and without the perforated diamond anvils and with the focusing optic at 1-ID in place is shown in Fig. 4.

## 4. Case study: nano-crystalline FeS at high *P*

The composition FeS crystallizes in two modifications, the mackinawite and troilite structures (Fig. 5). The first step in the formation of iron sulfides under hydrothermal conditions

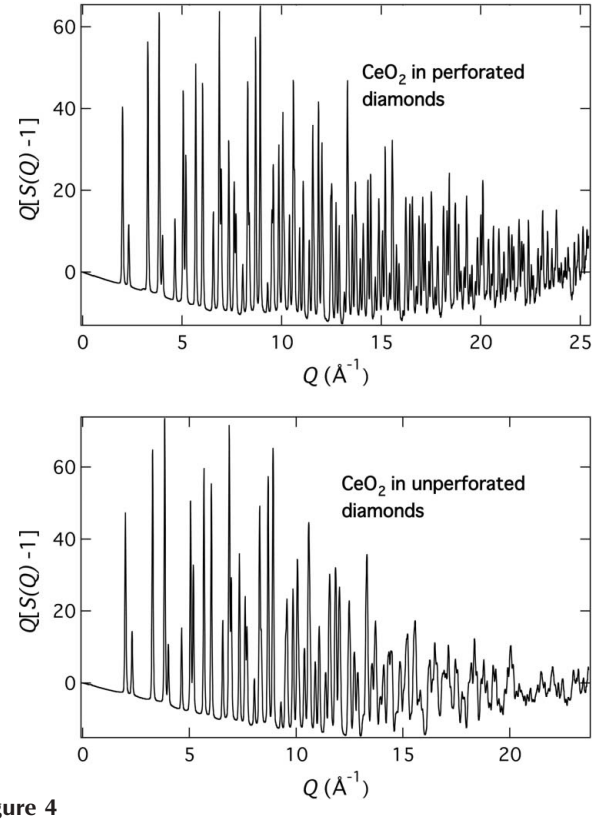


**Figure 4**
Diagrams showing $Q[S(Q) - 1]$ for nano-$CeO_2$ in (top) a cell fitted with perforated diamonds (Fig. 3) and (bottom) a standard diamond anvil cell. There is a dramatic decrease in the contribution to the overall scattering from diamonds in the perforated cell and this leads to a much better signal-to-noise discrimination at high $Q$, an important factor in deriving better resolved real-space correlation functions containing fewer 'ripples' owing to Fourier termination errors.

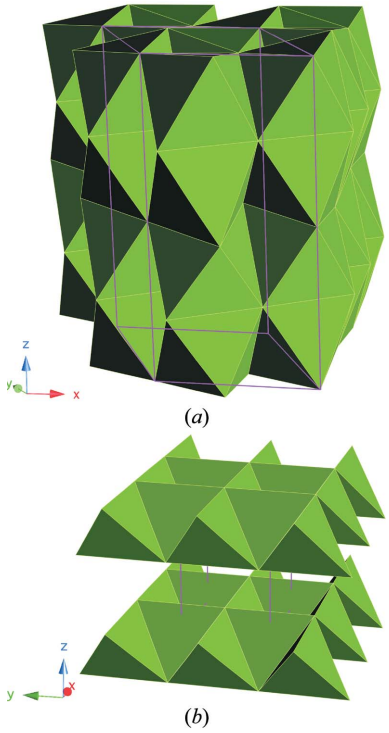


**Figure 5**
Representations of the structures of FeS polymorphs (*a*) troilite and (*b*) mackinawite. Iron sulfide polyhedra, octahedral and tetrahedral for troilite and mackinawite, respectively, are shown with iron at their approximate centers and sulfurs at the corners.

is the nucleation of a reduced short-range-ordered iron monosulfide (nano-FeS) that is generally believed to be a precursor to crystalline mackinawite. Using the total scattering technique we recently confirmed (Figs. 1 and 6) that nano-FeS is nano-crystalline with a particle size of about 4 nm, that it is single phase and that its PDF can be modelled using the mackinawite structure shown in Fig. 5 (Michel *et al.*, 2005).

The high-*P* behavior of nano-FeS is unknown. Since it is single phase, can be made reproducibly in the nano-crystalline form, and does not require the use of capping agents for stabilization, we thought it an excellent candidate material to explore the differences in high-*P* behavior between bulk crystalline and nano-crystalline materials. The high-*P* behavior of the troilite phase (Fig. 5) is summarized by Nelmes *et al.* (1999) and Marshall *et al.* (2000). Briefly, at room temperature troilite transforms at about 4.6 and 7.2 GPa to the so-called MnP and FeS-III modifications, respectively (Marshall *et al.*, 2000; Nelmes *et al.*, 1999). These three modifications are easily distinguished in the case where highly crystalline troilite is used as a starting material. All three polymorphs possess structures related to the NiAs-type (Fig. 5) and are distinguished by the presence of superlattice reflections resulting from atomic displacements from positions in the aristotype NiAs-related phase; in the case of neutron scattering (Marshall *et al.*, 2000) the differences are even more obvious as the transitions to MnP and FeS-III are accompanied by changes in the long-range magnetic order resulting in large changes in magnetic scattering at low *Q*.

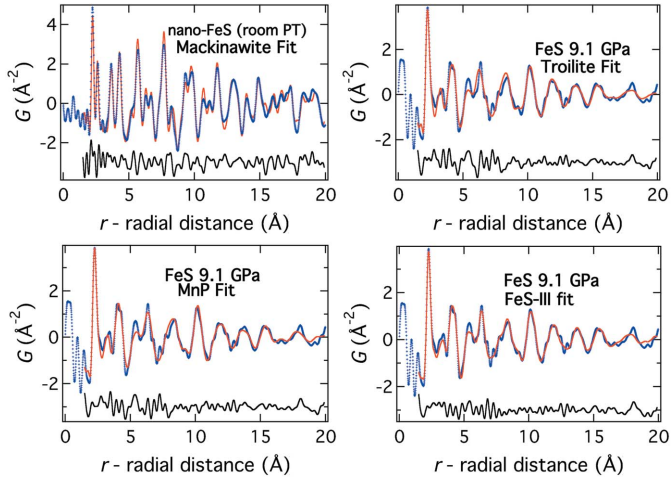


**Figure 6**
Diagrams showing fits to $G(r)$ for nano-crystalline FeS (mackinawite) at room $P$ and $T$ (top left) and the fit to $G(r)$ obtained from data collected at 9.1 GPa (Fig. 7) using the model for troilite (top right), the stable phase at ambient $P$ for bulk FeS shown in Fig. 5(*a*), and using the model for the MnP-related form (bottom left) and FeS-III (bottom right), the stable phase above about 4.6 GPa and 7.2 GPa, respectively (Nelmes *et al.*, 1999; Marshall *et al.*, 2000). The experimentally determined $G(r)$ in each case is shown as a blue dotted line and the model as a red continuous line. The difference curve (black line) is plotted below and on the same scale as the experimental and model-derived curves.

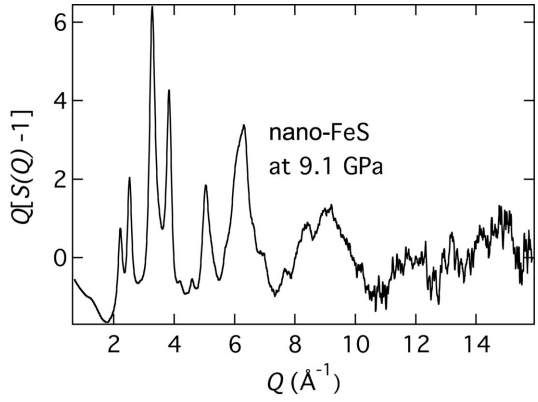


**Figure 7**
$Q[S(Q) - 1]$ *versus* $Q$ (Å$^{-1}$) for nano-crystalline FeS at 9.1 GPa.

For nano-crystalline mackinawite, sharp features in the diffraction pattern (Fig. 7) collected at 9.1 GPa using the protocols described above, occur at positions expected for the sub-lattice reflections of the NiAs-related phases, troilite, MnP-type and FeS-III, suggesting that the coordination number of iron has increased from 4 to 6 (Fig. 5). As expected, attempts to fit mackinawite- and troilite-related models (Fig. 6) to these data were unsuccessful. At this *P* we would expect FeS-III to be the stable polymorph of FeS and indeed this structure (Marshall *et al.*, 2000; Nelmes *et al.*, 1999) provides a better fit to the data than either troilite or the MnP-related structure (Fig. 6). The differences between the fits for MnP-type and FeS-III models, however, are subtle and underscore the need for the collection of the highest possible quality data.

## 5. Conclusion and future studies

Recent developments in focused high-energy beams, and modified diamond geometries, suggest quantitative data suitable for PDF analysis and the derivation of refined structure models can be obtained from samples at high $P$, in the DAC and other pressure vessels. It remains for the near future to rigorously test the suitability of the QHP-PDF technique for distinguishing between closely related models such as those, for example, related to the same aristotype. Several important classes of nano-materials fall into this category including those related to perovskite. It is clear at this early stage, however, that the strategies outlined above are suitable for a wide range of high-$P$ studies in DACs. The promise of our earlier work on crystalline samples of gold (Martin *et al.*, 2005) is partially fulfilled. Studies of lighter scatterers, such as silica and ice and glassy materials will be more challenging. It will be important to optimize the experiment by balancing $Q$-space resolution, minimizing Compton and other parasitic scattering from the pressure vessel, and maximizing the signal from the sample.

The X-ray diffraction data presented here were collected at beamline 1-ID of the Advanced Photon Source. Use of the Advanced Photon Source was supported by the US Department of Energy, Office of Science, Office of Basic Energy Sciences, under Contract No. W-31-109-Eng-38. We wish to thank GSECARS at sector 13 for use of high-pressure preparation facilities. JBP is grateful for the support of NSF through its DMR-0452444 and CHE-0221934 (CEMS) programs and to many collaborators at the aforementioned facility. The saw-tooth silicon refractive lenses were provided by C. Ribbing (Uppsala University, Sweden) and B. Cederstrom (Royal Institute of Technology, Sweden). Fig. 3 was provided by D'Anvils Ltd.

## References

Billinge, S. J. L. (2004). *Z. Kristallogr.* **219**, 117–121.
Cederstrom, B., Lundqvist, M. & Ribbing, C. (2002). *Appl. Phys. Lett.* **81**, 1399–1401.
Chen, B., Penwell, D., Benedetti, L. R., Jeanloz, R. & Kruger, M. B. (2002). *Phys. Rev. B*, **66**, 144101.
Chen, J., Parise, J. B., Li, R., Weidner, D. J. & Vaughan, M. (1998). *Proceedings of the US–Japan Seminar on 'Properties of Earth and Planetary Materials at High Pressure and Temperature'*, edited by M. Manyani and T. Yagi, pp. 139–144. Maui, Hawaii: AGU Monograph.
Chen, J., Weidner, D. J., Parise, J. B., Vaughan, M. T. & Raterron, P. (2001). *Phys. Rev. Lett.* **86**, 4072–4075.
Chen, J., Weidner, D. J., Vaughan, M. T., Parise, J. B., Zhang, J. & Xu, Y. (2000). *A Combined CCD/IP Detection System for Monchromatic XRD Studies at High Pressure and Temperature, Science and Technology of High Pressure*, edited by M. H. Manghnani, W. J. Nellis and M. F. Nicol, pp. 1035–1038. Hyderabad, India: Universities Press.
Chupas, P. J., Qiu, X. Y., Hanson, J. C., Lee, P. L., Grey, C. P. & Billinge, S. J. L. (2003). *J. Appl. Cryst.* **36**, 1342–1347.
Dadashev, A., Pasternak, M. P., Rozenberg, G. K. & Taylor, R. D. (2001). *Rev. Sci. Instrum.* **72**, 2633–2637.
Egami, T. & Billinge, S. J. L. (1994). *Underneath the Bragg Peaks: Structural Analysis of Complex Materials.* Oxford: Pergamon Press.
Egami, T. & Billinge, S. J. L. (2003). *Underneath the Bragg Peaks: Structural Analysis of Complex Materials.* Oxford: Elsevier.
Eggert, J. H., Weck, G., Loubeyre, P. & Mezouar, M. (2002). *Phys. Rev. B*, **65**, 174105.
Hammersley, A. P., Svensson, S. O., Hanfland, M., Fitch, A. N. & Hausermann, D. (1996). *High Press. Res.* **14**, 235–248.
Jorgensen, J. D., Hu, Z., Teslic, S., Argyriou, D. N., Short, S., Evans, J. S. O. & Sleight, A. W. (1999). *Phys. Rev. B*, **59**, 215–225.
Larson, A. C. & Von Dreele, R. B. (2000). Los Alamos National Laboratory Report 86–748. LANL, Los Alamos, NM, USA.
Lipinska-Kalita, K. E., Chen, B., Kruger, M. B., Ohki, Y., Murowchick, J. & Gogol, E. P. (2003). *Phys. Rev. B*, **68**, 035209.
Marshall, W. G., Nelmes, R. J., Loveday, J. S., Klotz, S., Hamel, G., Besson, J. M. & Parise, J. B. (2000). *Phys. Rev. B*, **61**, 11201–11204.
Martin, C. D., Antao, S. M., Chupas, P. J., Lee, P. L., Shastri, S. D. & Parise, J. B. (2005). *Appl. Phys. Lett.* **86**, 0619101–0619103.
Mezouar, M., Faure, P., Crichton, W., Rambert, N., Sitaud, B., Bauchau, S. & Blattmann, G. (2002). *Rev. Sci. Instrum.* **73**, 3570–3574.
Michel, F. M., Antao, S. M., Chupas, P. J., Lee, P. L., Parise, J. B. & Schoonen, M. A. A. (2005). *Chem. Mater.* Submitted.
Nelmes, R. J., McMahon, M. I., Belmonte, S. A. & Parise, J. B. (1999). *Phys. Rev. B*, **59**, 9048–9052.
Parise, J. B. (2004). *Structure Maps for Constrained Structures at High Pressures from Powder Diffraction: Practical Considerations and Case Studies*, Vol. 140, *School on High Pressure Crystallography*, edited by A. Katrusiak and P. M. McMillan, pp. 37–56. Erice, Italy, 4–15 June 2004. Dordrecht: Kluwer.
Petkov, V., Jeong, I. K., Chung, J. S., Thorpe, M. F., Kycia, S. & Billinge, S. J. L. (1999). *Phys. Rev. Lett.* **83**, 4089–4092.
Petkov, V., Trikalitis, P. N., Bozin, E. S., Billinge, S. J. L., Vogt, T. & Kanatzidis, M. G. (2002). *J. Am. Chem. Soc.* **124**, 10157–10162.
Proffen, T. & Billinge, S. J. L. (1999). *J. Appl. Cryst.* **32**, 572–575.
Proffen, T., DiFrancesco, R. G., Billinge, S. J. L., Brosha, E. L. & Kwei, G. H. (1999). *Phys. Rev. B*, **60**, 9973–9977.
Qiu, X., Thompson, J. W. & Billinge, S. J. L. (2004). *J. Appl. Cryst.* **37**, 678.
Shastri, S. D. (2004). *J. Synchrotron Rad.* **11**, 150–156.
Shastri, S. D., Fezzaa, K., Mashayekhi, A., Lee, W.-K., Fernandez, P. B. & Lee, P. L. (2002). *J. Synchrotron Rad.* **9**, 317–322.
Shen, G. Y., Prakapenka, V. B., Rivers, M. L. & Sutton, S. R. (2003). *Rev. Sci. Instrum.* **74**, 3021–3026.
Toby, B. H. (2001). *J. Appl. Cryst.* **34**, 210–213.
Wang, Z. W. & Saxena, S. K. (2002). *Solid State Commun.* **123**, 195–200.
Wang, Z. W., Saxena, S. K., Pischedda, V., Liermann, H. P. & Zha, C. S. (2001*a*). *J. Phys. Condens. Matter*, **13**, 8317–8323.
Wang, Z. W., Saxena, S. K., Pischedda, V., Liermann, H. P. & Zha, C. S. (2001*b*). *Phys. Rev. B*, **64**, 012102.
Wasada, Y. (1980). *The Structure of Noncrystalline Materials.* New York: McGraw-Hill.
Xu, J., Mao, H. K., Hemley, R. J. & Hines, E. (2002). *J. Phys. Condens. Matter*, **14**, 11543–11548.
Zhao, Y. S., Parise, J. B., Wang, Y. B., Kusaba, K., Vaughan, M. T., Weidner, D. J., Kikegawa, T., Chen, J. & Shimomura, O. (1994). *Am. Mineral.* **79**, 615–621.